RadioGraphics

Dual-Energy CT with Single- and Dual-Source Scanners: Current Applications in Evaluating the Genitourinary Tract[1]

Ravi K. Kaza, MD • Joel F. Platt, MD • Richard H. Cohan, MD • Elaine M. Caoili, MD • Mahmoud M. Al-Hawary, MD • Ashish Wasnik, MD

ONLINE-ONLY CME

See www.rsna.org/education/rg_cme.html

LEARNING OBJECTIVES

After completing this journal-based CME activity, participants will be able to:

- Describe the use of dual-energy CT with fast kilovoltage switching to obtain material-specific information for genitourinary diagnoses.
- Explain the value of virtual unenhanced images obtained with dual-energy CT for characterizing renal masses and for CT urography.
- List the current limitations of dual-energy CT for genitourinary applications.

TEACHING POINTS

See last page

Several promising clinical applications for dual-energy computed tomography (CT) in genitourinary imaging have been reported. Dual-energy CT not only provides excellent morphologic detail but also can supply material-specific and quantitative information that may be particularly useful in genitourinary imaging. Dual-energy CT has unique capabilities for characterizing renal lesions by quantifying iodine content and helping identify the mineral contents of renal stones, information that is important for patient care. Virtual unenhanced images reconstructed from dual-energy CT datasets can be useful for detecting calculi within the iodine-filled urinary collecting system, potentially reducing the need for an unenhanced scanning phase at CT urography. Although the underlying principles of dual-energy CT are the same regardless of scanner type, single-source dual-energy scanners with fast kilovoltage switching differ from dual-source dual-energy scanners both in image data acquisition and in processing methods; an understanding of these differences may help optimize dual-energy CT genitourinary protocols. Dual-energy CT performed with a dual-source scanner or with a single-source scanner with fast kilovoltage switching also has some important limitations. Further advances in scanning protocols and refinement of processing techniques to reduce image noise may lead to more widespread use of dual-energy CT.

RadioGraphics 2012; 32:353–369 • **Published online** 10.1148/rg.322115065 • **Content Codes:** CT GU PH

[1]From the Department of Radiology, University of Michigan Hospitals, 1500 E Medical Center Dr, UH B1 D 502 E, Ann Arbor, MI 48109. Recipient of a Certificate of Merit award for an education exhibit at the 2010 RSNA Annual Meeting. Received March 30, 2011; revision requested May 9 and received June 13; accepted July 11. For this journal-based CME activity, the authors R.K.K., J.F.P, and R.H.C. have disclosed various financial relationships (see p 368); all other authors, the editor, and reviewers have no relevant relationships to disclose. **Address correspondence to** R.K.K. (e-mail: *ravikaza@med.umich.edu*).

Introduction

The concept of dual-energy computed tomography (CT) originated during the early development of CT (1–3). However, it was only recently that advances in scanner technology made dual-energy CT possible for routine clinical use (4,5). With the increasing availability of dual-energy CT scanners, several clinical applications have been investigated, including the characterization of renal masses and stones (6–9). Most of the literature about genitourinary applications of dual-energy CT is based on the use of dual-source dual-energy CT scanners (5,7,10). However, dual-energy CT also can be performed with a single-source scanner that relies on fast kilovoltage switching, a technique that differs from dual-source dual-energy CT in both image data acquisition and processing methods but that has similar applications.

The article describes the salient features of available dual-energy CT scanners and image processing, emphasizing the important differences between single-source dual-energy CT with fast kilovoltage switching and dual-source dual-energy CT. Current applications and limitations of dual-energy CT for CT urography generally, and for the characterization of renal masses and renal stones specifically, are explained.

Principles of Dual-Energy CT

Conventional (single-energy) CT is performed at a fixed tube potential. On the conventional CT scanner console, x-ray attenuation quantified in Hounsfield units is represented in shades of gray. Images obtained with conventional CT provide useful structural information but only limited material-specific information because the representation of structures on these images depends solely on the linear attenuation coefficient of each of the constituent materials and is independent of the material density and mass-attenuation coefficient.

Teaching Point

With dual-energy CT, two image datasets are acquired in the same anatomic location with two different x-ray spectra to allow the analysis of energy-dependent changes in the attenuation of different materials (1). Each type of material demonstrates a relatively specific change in attenuation between images obtained with a high-energy spectrum and those obtained with a low-energy spectrum, and this attenuation difference allows a more nuanced characterization of the features depicted. Two different materials that show similar attenuation on images acquired with one of the two energy spectra are often more easily differentiated on images acquired with the other spectrum because of substantial differences in their attenuation (Fig 1). For example, although iodine and calcium may demonstrate similar attenuation on conventional CT images, the attenuation of iodine increases more markedly than that of calcium on dual-energy CT images obtained with low energy when compared with images obtained with high energy (3), and this attenuation difference facilitates differentiation of the two materials.

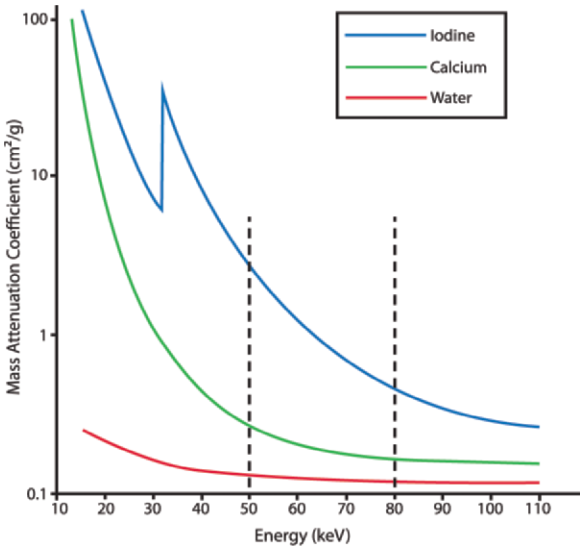

Figure 1. Graph of mass-attenuation coefficients for iodine (blue), calcium (green), and water (red) on CT images obtained at two different energies (vertical dashed lines) shows that these materials can be characterized by comparing their attenuation at the lower energy with that at the higher energy. When dual-energy images reconstructed for 50 and 80 keV are compared, iodine demonstrates a greater decrease in attenuation than calcium does at the higher energy, whereas the attenuation of water remains more or less constant.

Dual-Energy CT Scanners

Three types of dual-energy CT scanners are available that differ in the technique used to acquire high- and low-energy CT datasets: a dual-source dual-energy scanner, a single-source dual-energy scanner with fast kilovoltage switching (ie, rapid alternation between high and low kilovoltage settings), and a single-source dual-energy scanner with dual detector layers.

Dual-Source Scanner with Dual Detector Arrays

On the dual-source scanner (Somatom Definition; Siemens, Forchheim, Germany), two separate detector arrays acquire two different image datasets from two separate x-ray tubes operating at two different tube potentials (11). High-energy scans are obtained at 120 or 140 kVp, and low-energy scans are obtained simultaneously at 80 or 100 kVp (5,11). The use of two separate x-ray sources allows beam filtration and adjustment of the current in each tube in order to optimize image quality. Dual-source dual-energy CT images are somewhat limited in temporal registration because the high- and low-energy datasets are obtained at slightly different times. Furthermore, the limited (33-cm) field of view available for use in image analysis could impede evaluation of the entirety of some abdominal organs in patients with a large body habitus.

Single-Source Scanner with Fast Kilovoltage Switching

This single-source CT scanner with a single detector layer (Discovery CT 750HD; GE Healthcare, Milwaukee, Wis) relies on a single x-ray source with fast switching between two kilovoltage settings (80 and 140 kVp) at intervals of 0.5 msec during a single gantry rotation to generate high- and low-energy x-ray spectra (12). The tube current cannot be altered simultaneously; it remains constant during both high- and low-energy acquisitions. To account for the higher tube output at 140 kVp, the exposure time ratio is varied between the 80-kVp and the 140-kVp acquisitions to maximize the contrast-to-noise ratio: typically, 65% of the exposure time is used for the 80-kVp acquisition, and 35%, for the 140-kVp acquisition (13). A detector with a fast response and a data acquisition system with a fast sampling capability are used to capture the alternating high- and low-energy data (12). The advantages of dual-energy CT with fast kilovoltage switching are good temporal registration between high- and low-energy datasets, which are obtained nearly simultaneously, and the availability of the full 50-cm field of view for use in image analysis. However, because a single x-ray source is used, individual modification of the high- and low-energy x-ray beams is difficult (not yet possible on commercially available scanners), and spectral overlap is increased.

Single-Source Scanner with Dual Detector Layers

The prototype for another single-source dual-energy CT scanner (Brilliance CT; Philips Healthcare, Andover, Mass) has a modified detector array with two scintillation layers arranged one atop the other to receive separate high- and low-energy image data streams from a single x-ray source (14). The bottom detector layer captures high-energy data, and the top layer captures low-energy data; from these two datasets, two separate image series are reconstructed (14,15). This dual-energy CT scanner is not yet available for routine clinical use.

Dual-Energy CT Image Reconstruction

For optimal clinical benefit, images generated from dual-energy CT datasets should provide structural information similar to that provided by conventional single-energy CT scans; in addition, they can provide material-specific information. To obtain material-specific information, the dual-energy datasets are processed either after the reconstruction of high- and low-energy images (in image-domain decomposition) or before images are reconstructed from high- and low-energy sinograms (in data-domain or projection-space decomposition) (16). Image-domain decomposition is used for material analysis of images obtained with a dual-source or dual-layer dual-energy CT scanner, whereas data-domain decomposition is used for material analysis of dual-energy CT images obtained with fast kilovoltage switching. Projection-space decomposition is preferred because it enables greater flexibility in material decomposition and permits the preprocessing correction of data to minimize beam-hardening artifacts (17).

When dual-energy CT is performed with fast kilovoltage switching, the 140-kVp images are reconstructed immediately at the scanner console. These images are not fully corrected for scanner calibration and are used only to verify the adequacy of anatomic coverage. To facilitate workflow and reduce scanner processing time, 80-kVp images are not routinely reconstructed. If needed, information similar to that provided by the 80-kVp images can be obtained from the lower-energy monochromatic images after processing. Calibration corrections are applied

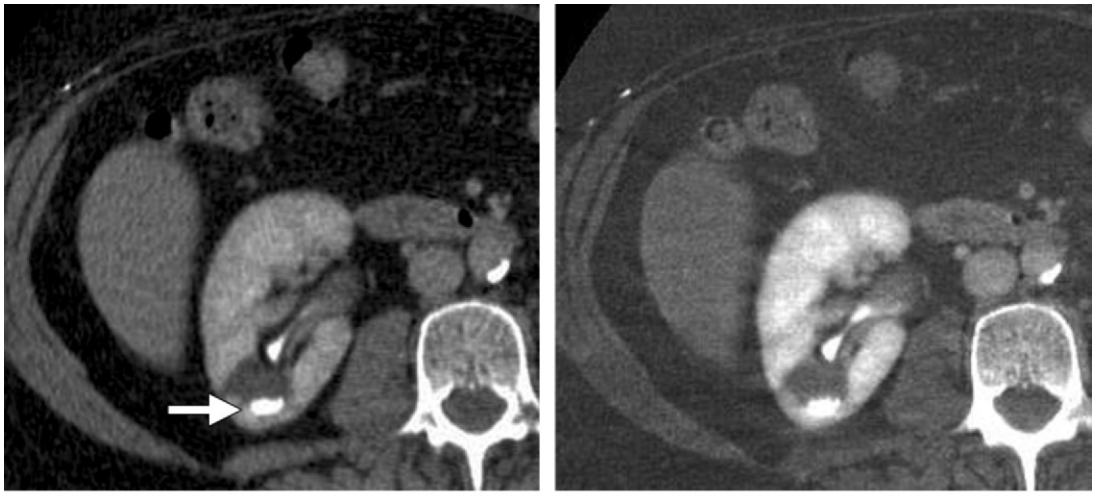

a. b.

c.

Figure 2. **(a)** Axial contrast-enhanced dual-energy CT scan shows a 2-cm cystic lesion in the right kidney with high-attenuation material along its dependent portion (arrow). **(b, c)** Paired iodine-density **(b)** and water-density (virtual unenhanced) **(c)** images, generated from the same dual-energy CT dataset as in **a** by using an iodine-water basis material decomposition algorithm, show calcium in bone, in the renal cyst, and in the aortic wall. Calcium is depicted on both images in the iodine-water pair because the iodine-water decomposition algorithm treats calcium as though it were composed of both basis materials, since the attenuation of calcium resembles neither that of iodine nor that of water.

to the high- and low-energy datasets, which are aligned in projection space and transformed into material-basis pair projections, which are then used to reconstruct two main types of images: *(a)* material-density images, which provide material-specific information, and *(b)* monochromatic images, which provide energy-selective information (12).

Teaching Point

The generation of material-density images is based on the theory of basis material decomposition, which proposes that the attenuation coefficients of any material can be computed as a weighted sum of the attenuation coefficients of two basis materials as long as the k-edge of the material is not within the evaluated energy range (1,3). The two basis materials should have substantially different mass-attenuation coefficients; thus, the material pairs chosen usually differ greatly in effective atomic number. On the material-density images, substances other than the chosen basis materials are considered to contain combinations of both selected material densities. Two sets of material-density images are then generated, each demonstrating the presence or absence of each basis material selected (Fig 2). Two commonly selected dual-energy CT basis material pairs are *(a)* iodine and calcium and *(b)* iodine and water. When iodine (which has a high atomic number) is paired with water (which has a low atomic number), two separate sets of

images (a set of iodine-density images and a set of water-density images) are generated. On the water-density image in an iodine-water image pair generated from the contrast material–enhanced dual-energy CT dataset, voxels that show an energy-dependent change in attenuation resembling the attenuation of iodine are removed and represented instead on the iodine-density image. The virtual unenhanced images thus generated from the contrast-enhanced dual-energy dataset can provide information equivalent to that obtainable from unenhanced images obtained before the administration of contrast material. The iodine-density images of the material-density image series are used to assess structures for areas of enhancement. Only lesions that contain iodine will show higher density (ie, appear brighter) on iodine-density images than they do on water-density images.

Unlike image data generated by single-energy CT at a single peak voltage, dual-energy CT image data can be processed to obtain images at any specified single photon energy. Such images are commonly described as monochromatic, although a more appropriate description might be *pseudomonochromatic* because the images are generated by calculating energy-selective monochromatic projection data from dual-energy CT data (18). Monochromatic projections for any photon energy can be generated during the processing of material-density image data by calculating the linear attenuation coefficient (μ) of an object so that the attenuation characteristics of the object are exactly as they would be if the object were imaged with a monochromatic beam at the specified photon energy (19). Because monochromatic dual-energy CT images are generated from projection-space data, they are less affected by beam-hardening artifact and provide more accurate CT numbers than do standard single-energy CT images. These advantages can improve the characterization of renal lesions by decreasing pseudoenhancement (artifactual increase in CT numbers) in simple renal cysts and thus reducing the likelihood that cysts will be mistaken for solid lesions (20). In addition, because monochromatic dual-energy CT images can be generated for any photon energy level between 40 and 140 keV, a set of images can be created that optimizes contrast differences between two adjacent structures, such as a renal mass and normal renal parenchyma. Decreasing the photon energy level from 140 keV to 40 keV increases the attenuation of iodine and produces an associated increase in image noise. Monochromatic dual-energy CT images generated at a photon energy level of 60–75 keV have been reported to demonstrate a peak contrast-to-noise ratio and, because they contain less image noise, to allow a more reliable interpretation (13,21).

Image data processing techniques for dual-source dual-energy CT are described in detail in several published reports (4,5,22). With dual-source dual-energy CT, images for diagnostic interpretation are generated by linear or nonlinear sigmoidal blending of high- and low-energy image datasets (5). Material-specific images are generated by measuring the differences in attenuation of various materials between the low-energy and high-energy image datasets and either highlighting the pixels corresponding to the selected material or subtracting the pixels corresponding to the other materials. For abdominal imaging applications, a three-material (soft tissue, fat, and iodine) decomposition process is usually used to generate virtual unenhanced images (4,23). A color-coded overlay image also can be generated from dual-energy data; this type of image enables visualization of the distribution of a selected material across the entire CT volume (6). A color-coded overlay image is generated by assigning a color to the voxels containing the selected material and superimposing those voxels on monochromatic images in the same volume location to facilitate anatomic correlation. For abdominal applications, iodine overlay images from dual-energy CT are especially useful for depicting enhancement within a lesion.

The relative advantages and disadvantages of the three types of dual-energy scanners are summarized in the Table. Because dual-energy CT involves the acquisition and storage of two different energy datasets, the amount of data obtained in each CT examination is substantially increased. Thus, image archive servers with a large storage capacity are needed, and advanced computational

Relative Advantages and Disadvantages of Different Dual-Energy CT Systems

Scanner Type	Hardware Description	Advantages	Disadvantages
Dual-source dual-energy CT	Two x-ray sources, two detectors	Good spectral separation between high- and low-energy scans; easy to equalize dose and noise between high- and low-energy scans by modulating tube current for each tube; attenuation in Hounsfield units can be measured on virtual unenhanced images	Limited temporal and spatial registration because two separate image datasets are acquired; maximum field of view for dual-energy acquisition is 33 cm; image-domain dual-energy decomposition limits flexibility
Dual-energy CT with fast kilovoltage switching	Single x-ray source, single detector	Good temporal and spatial registration; projection-space dual-energy decomposition offers greater flexibility; easy quantification of iodine density; 50-cm field of view	Limited spectral separation between high- and low-energy scans; higher noise on images obtained with lower peak voltage (because tube current cannot be modulated at the same time the peak voltage is altered); inability to measure attenuation on virtual unenhanced images
Multilayered-detector dual-energy CT	Single x-ray source, dual detector layers	Perfect temporal and spatial registration; projection-space dual-energy decomposition can be used	Limited energy separation with substantial spectral overlap

software is required for image analysis and interpretation. In addition, the attenuation measurements that help identify fat, water, and contrast enhancement on single-energy 120-kVp scans are not fully applicable when interpreting features on monochromatic images and blended images generated from dual-energy image datasets; although these CT numbers are useful as guides, new reference standards specific to dual-energy CT are needed.

Quantitative Estimation

Two different types of clinically useful quantitative information can be generated at dual-energy CT with fast kilovoltage switching: *(a)* the physical densities of known basis material pairs (eg, iodine and water) and *(b)* the effective atomic number of a substance located in a selected region of interest.

The physical density of a material can be measured directly from material-density images (3). For example, by placing a region of interest over a lesion on iodine- and water-density images, the densities of iodine and water in the lesion can be measured in milligrams per milliliter. The density of iodine in a lesion also can be used to define and quantify lesion enhancement.

The effective atomic number of a compound represents the weighted average of the atomic numbers of constituent elements in the compound (24). If the constituent elements in a compound are known, the effective atomic number can be calculated from the ratio of the linear attenuation coefficients of elements in the compound at two different energies (μ_{high}/μ_{low}) (25). From the dual-energy CT dataset, images can be generated that enable measurement of the effective atomic number within a selected region of interest. Because different materials with similar attenuation measurements at a given energy can

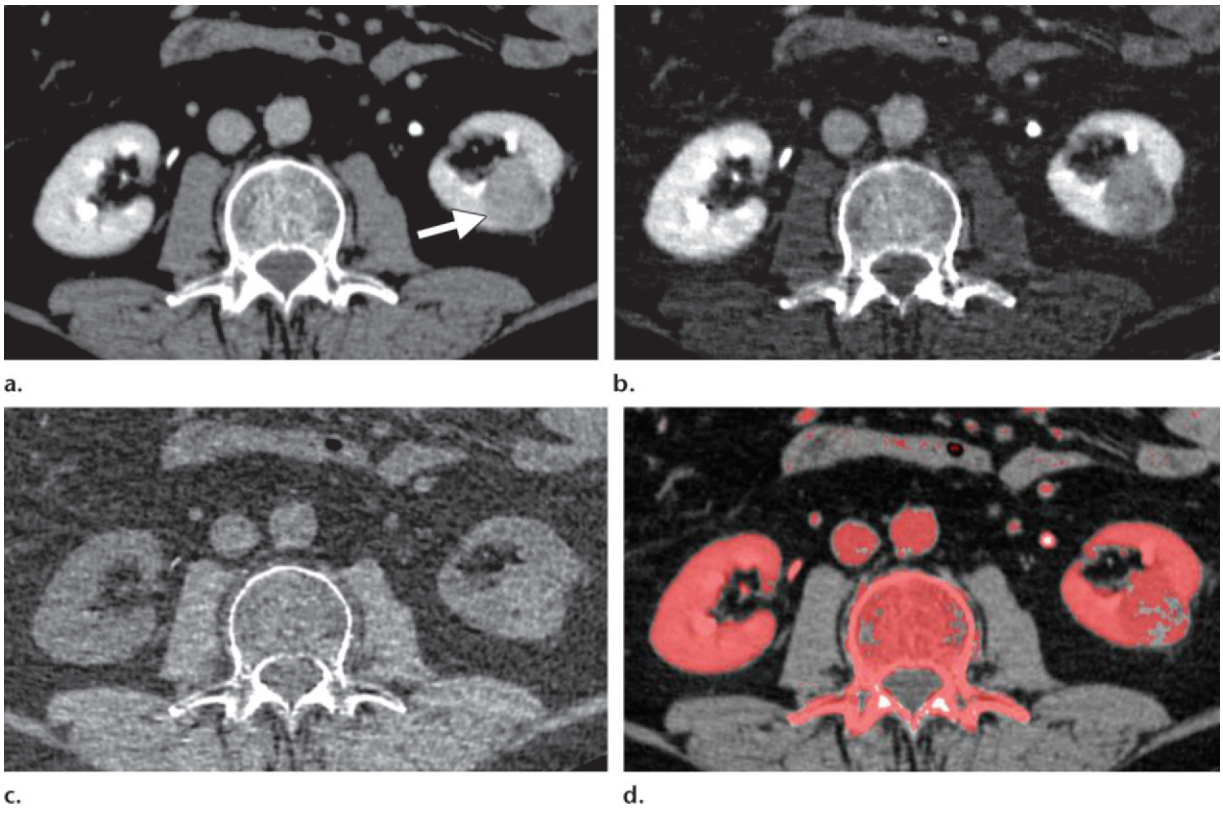

Figure 3. Soft-tissue mass. **(a)** Axial monochromatic 75-keV image from contrast-enhanced dual-energy CT shows a 3-cm heterogeneous left renal lesion (arrow). **(b)** Iodine-density image from an iodine-water material-density image pair obtained from the same dual-energy CT dataset as in **a** shows focal areas of increased brightness representing enhancement interspersed with darker areas in the lesion. **(c)** Water-density image from the same material-density image pair shows that the areas of the lesion that appear brighter in **b** are slightly hyperdense relative to the adjacent renal parenchyma, a finding indicative of soft tissue. **(d)** Color-coded iodine overlay image shows large iodine-containing regions (red pixels) within the lesion, findings suggestive of an enhancing solid mass.

have different effective atomic numbers, this application of dual-energy CT data may help improve material discrimination (25).

Renal Mass Characterization

Simple renal cysts, which have attenuation similar to that of water, are easily characterized on conventional CT images acquired with a single energy and a single contrast-enhanced scanning phase. However, reliable characterization of many hyperattenuating renal cysts and solid renal masses requires scanning with a protocol for renal masses, which includes an initial unenhanced scanning phase followed by contrast-enhanced scanning to allow the assessment of any change in lesion attenuation, with some investigators using an attenuation increase of at least 10 HU, and others, more than 20 HU, to define enhancement (26). Enhancement is the most important criterion for differentiating solid masses, which might require surgery, from benign cysts with proteinaceous or hemorrhagic contents, which might not require any follow-up (27).

Teaching Point

Paired iodine- and water-density images obtained at contrast-enhanced dual-energy CT with fast kilovoltage switching can help distinguish hyperattenuating cysts from enhancing masses without the need for an unenhanced scanning phase (Figs 3, 4) (28). On iodine-density images, voxels containing iodine appear bright, whereas

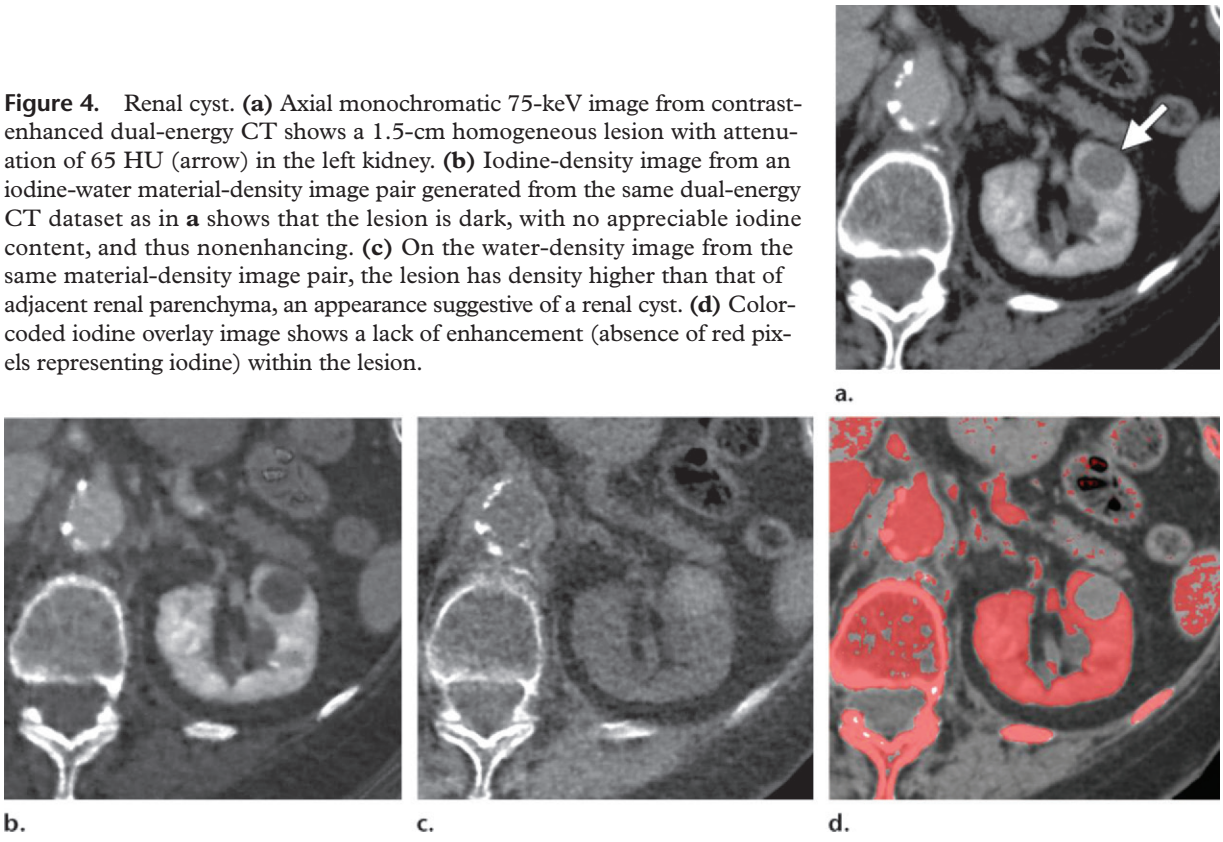

Figure 4. Renal cyst. **(a)** Axial monochromatic 75-keV image from contrast-enhanced dual-energy CT shows a 1.5-cm homogeneous lesion with attenuation of 65 HU (arrow) in the left kidney. **(b)** Iodine-density image from an iodine-water material-density image pair generated from the same dual-energy CT dataset as in **a** shows that the lesion is dark, with no appreciable iodine content, and thus nonenhancing. **(c)** On the water-density image from the same material-density image pair, the lesion has density higher than that of adjacent renal parenchyma, an appearance suggestive of a renal cyst. **(d)** Color-coded iodine overlay image shows a lack of enhancement (absence of red pixels representing iodine) within the lesion.

voxels that do not contain iodine appear dark, resembling the appearance of nonenhancing fat. The greater brightness of renal masses on iodine-density images helps distinguish them from nonenhancing cysts, even when their attenuation measurements on contrast-enhanced CT images are similar (Fig 5). Iodine density also can be quantitatively measured to differentiate enhancing renal lesions from nonenhancing ones (Fig 6) (28). Color-coded image overlays based on iodine density measurements in each pixel allow easy visualization of the presence or absence of enhancement.

In addition, water-density images may be used as virtual unenhanced images to allow the detection of calcification within a renal mass. Such calcification is often obscured by enhancement on conventional contrast-enhanced CT images. There is a difference between virtual unenhanced images obtained with dual-source dual-energy CT and those obtained with single-source dual-energy CT with fast kilovoltage switching: Dual-source dual-energy CT scanners use image-domain three-material decomposition and hence allow the measurement of lesion attenuation in Hounsfield units (7). By contrast, virtual unenhanced images generated by dual-energy CT scanners with fast kilovoltage switching provide lesion density measurements in milligrams per milliliter of water and do not allow attenuation measurements; although image processing algorithms exist that would allow the extrapolation of attenuation data in Hounsfield units from these images, scanners with such algorithms are not yet available for clinical use (29).

Both dual-source dual-energy CT and dual-energy CT with fast kilovoltage switching have a few technical limitations for the evaluation of renal masses. First, despite efforts that have been made to reduce image noise, virtual unenhanced images are noisier than real unenhanced images. Second, because of the material decomposition algorithms used, calcification in renal lesions is less conspicuous on virtual unenhanced images than on real unenhanced images. Third, although large accumulations of fat in renal masses are readily apparent on monochromatic

a.

b.

c.

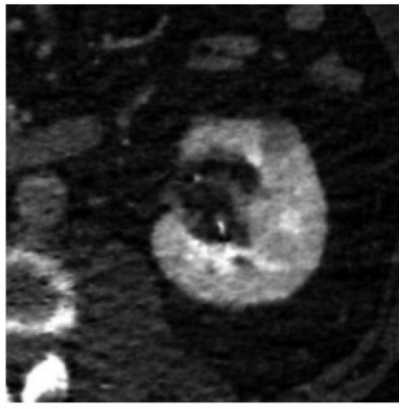

d.

Figure 5. **(a, b)** Axial monochromatic 75-keV images obtained with contrast-enhanced dual-energy CT at different levels show a 1.8-cm exophytic lesion with attenuation of 57 HU along the posterior aspect of the left kidney (arrow in **a**) and a 1.6-cm lesion with attenuation of 69 HU in the anterior part of the left kidney (arrowhead in **b**). **(c, d)** On iodine-density images from two iodine-water material-density image pairs generated from the same dual-energy CT datasets as in **a** and **b**, the posterior lesion has low density indicative of a lack of enhancement, whereas the anterior lesion has intermediate density indicative of mild enhancement. Despite the similar CT numbers of these two lesions on contrast-enhanced images, their iodine densities were markedly divergent: The iodine density of the posterior lesion was 0.84 mg/mL, whereas that of the anterior lesion was 2.9 mg/mL. The presence of a posterior left renal cyst and an anterior left renal mass was corroborated by the findings on conventional (single-energy) unenhanced and contrast-enhanced CT images.

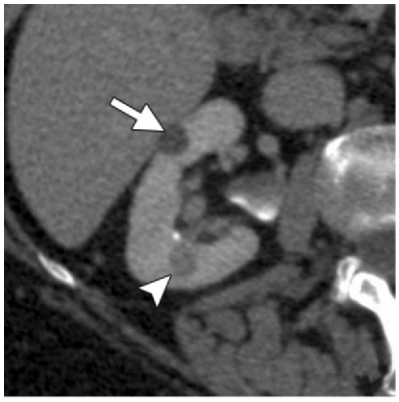

a.

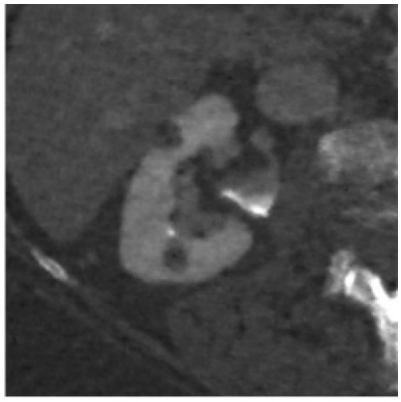

b.

Figure 6. **(a)** Axial monochromatic 75-keV image from contrast-enhanced dual-energy CT shows two lesions in the right kidney, each with a maximal diameter of 1 cm. The anterior lesion (arrow) has attenuation of 10 HU, a finding suggestive of a simple cyst, and the posterior lesion (arrowhead) has attenuation of 85 HU, a finding that might represent either a solid mass or a complex cystic lesion. **(b)** Iodine-density image from an iodine-water material-density image pair generated from the same dual-energy CT dataset as in **a** shows a dark appearance of both lesions, an indicator of lack of iodine content and, thus, nonenhancement. The measured iodine density in the anterior simple cyst was 0.9 mg/mL, and that in the posterior cyst was 0.95 mg/mL. Although the measured attenuation of the lesions differed substantially, neither lesion contained a substantial amount of iodine.

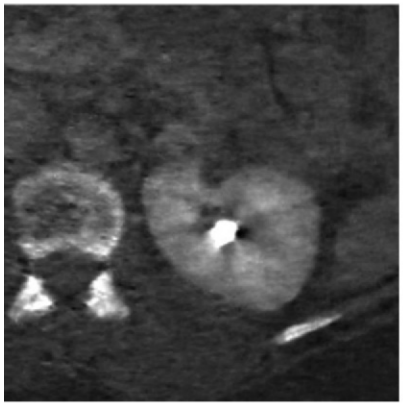

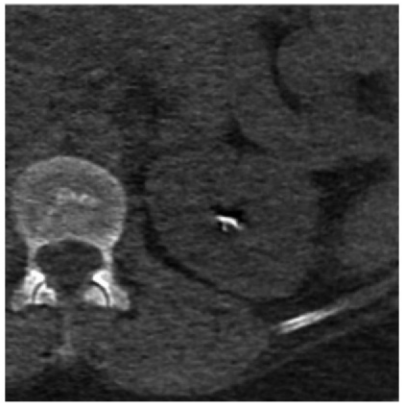

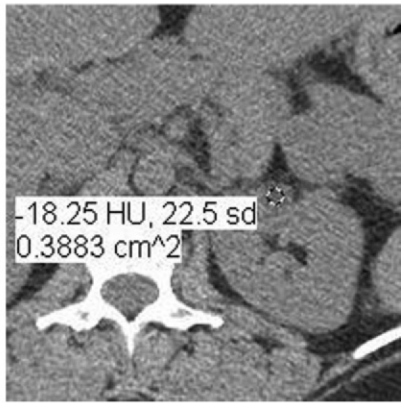

Figure 7. **(a)** Axial monochromatic 75-keV image from contrast-enhanced dual-energy CT shows a 1-cm lesion (arrow) with attenuation of 38 HU in the left kidney. **(b)** Iodine-density image from an iodine-water material-density image pair generated from the same dual-energy CT dataset as in **a** shows a dark appearance of the lesion, a finding suggestive of a nonenhancing renal cyst. **(c)** Water-density image from the same material-density image pair as **b** shows that the lesion is isodense, relative to the renal parenchyma. **(d)** Conventional unenhanced CT image shows attenuation of approximately –18 HU in the lesion, a finding suggestive of an angiomyolipoma. This case shows how the poor depiction of small amounts of fat on iodine- and water-density images could result in an inaccurate diagnosis of renal lesions if they are evaluated solely on the material-density images. *sd* = standard deviation.

images obtained from dual-energy CT with fast kilovoltage switching, smaller amounts of fat in renal masses are difficult to detect on virtual unenhanced images and can be measured only on conventional thin-section unenhanced CT images (Fig 7). Thus, when evaluating renal masses at dual-energy CT with fast kilovoltage switching, it may be necessary to obtain an additional series of fat-specific material-density images.

Follow-up after Thermal Ablation of Renal Masses

Thermal ablation of solid renal masses is usually performed in patients who are not surgical candidates. Follow-up imaging is often performed with CT to determine whether residual or recurrent tumor tissue is present. Post–thermal ablation CT usually involves scanning in multiple phases to detect any areas of enhancement that might be indicative of residual or recurrent tumor tissue within the ablation cavity (30). Dual-energy CT also can depict such enhancement, and because it involves a single phase of scanning, it may help limit the radiation dose received by the patient (Fig 8) (31).

Characterization of Renal Stones

Although unenhanced CT is still the reference standard for evaluating known or suspected urinary tract calculi, its utility for characterizing different types of calculi is limited because of frequent overlap in their attenuation measurements and because many calculi are of a mixed type (32). The different types of renal calculi, with their frequency of occurrence, include calcium-based stones (70%–80%) such as calcium oxalate monohydrate, calcium oxalate dihydrate, and calcium phosphate calculi; struvite (magne-

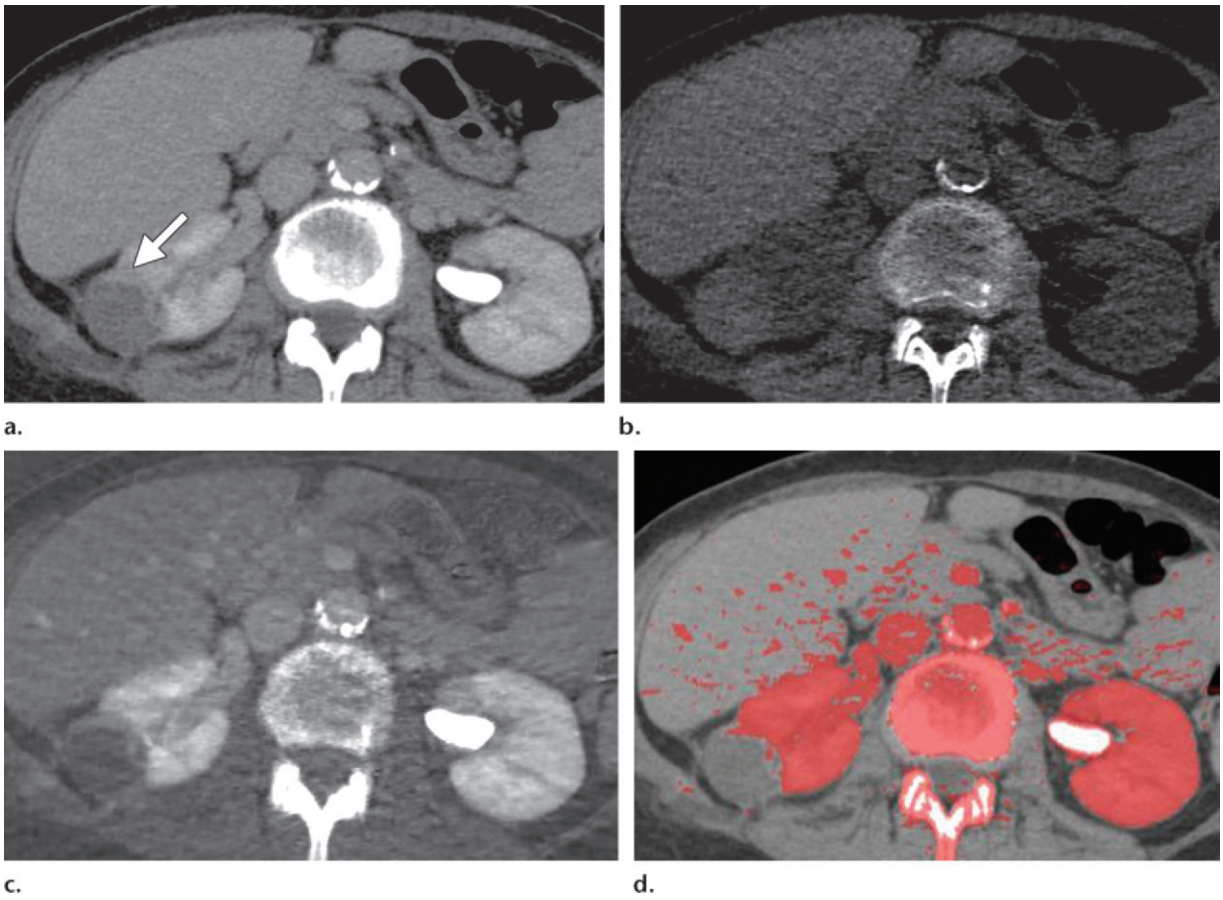

Figure 8. Follow-up imaging after radiofrequency ablation of a renal mass. **(a)** Axial monochromatic 75-keV image from dual-energy CT shows an ablation cavity (arrow) along the lateral aspect of the right kidney. Note the peripheral linear region of higher attenuation in the cavity. **(b)** Water-density image from an iodine-water material-density image pair generated from the same dual-energy CT dataset as in **a** shows hyperdensity of the ablation cavity in comparison with the renal parenchyma. **(c)** Iodine-density image from the same material-density image pair as **b** shows a predominantly dark appearance suggestive of nonenhancement in a large portion of the ablation cavity. However, a thin anterior rim of higher density is suggestive of enhancement due to iodine content and, thus, of tumor recurrence. **(d)** Iodine overlay image shows color-coded pixels indicative of iodine content within the thin rim of tissue along the anterior aspect of the ablation cavity, adjacent to enhancing normal renal parenchyma.

sium ammonium phosphate) stones (5%–15%); uric acid stones (5%–10%); and cystine stones (1%–2.5%). Knowledge about the composition of stones may guide decisions about their management and shape expectations concerning the effectiveness of therapy. For example, uric acid calculi can be managed with oral medications that facilitate dissolution, and struvite calculi are amenable to extracorporeal shock-wave lithotripsy, whereas calcium oxalate monohydrate and cystine calculi are relatively resistant to fragmentation with lithotripsy (32).

Teaching Point

At dual-energy CT, the change in attenuation between high- and low-energy scans can be used to differentiate types of calculi, some of which might have a similar attenuation when scanned at a single energy level (33). The results of initial studies evaluating the effectiveness of dual-source dual-energy CT for characterizing urinary tract calculi are promising. In particular, dual-energy CT has helped distinguish uric acid–containing calculi from non–uric acid–containing

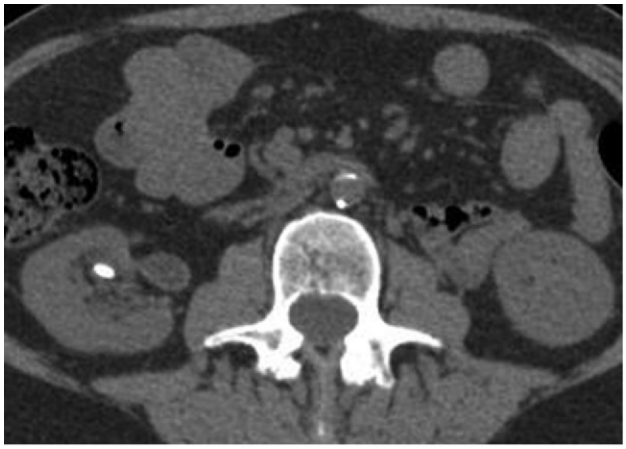

9a.

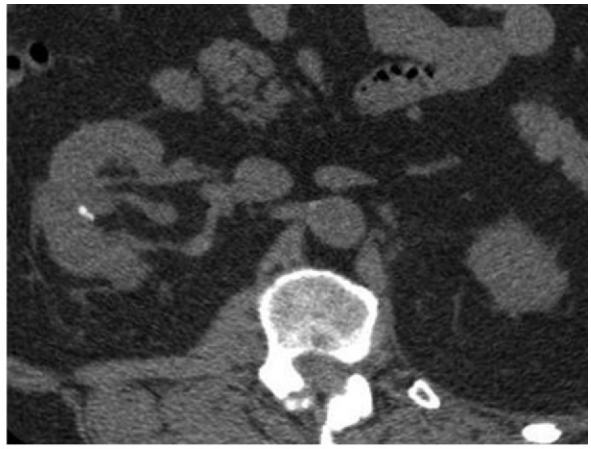

10a.

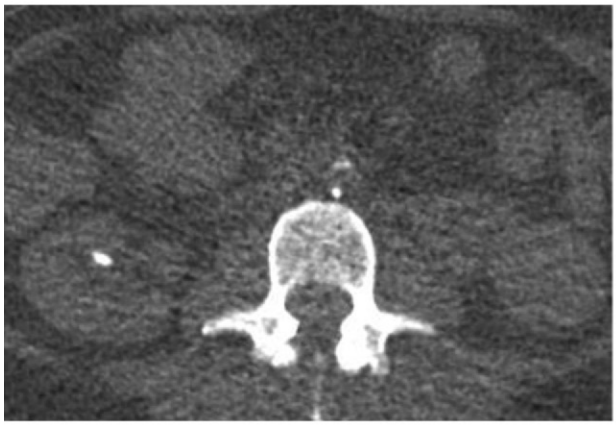

9b.

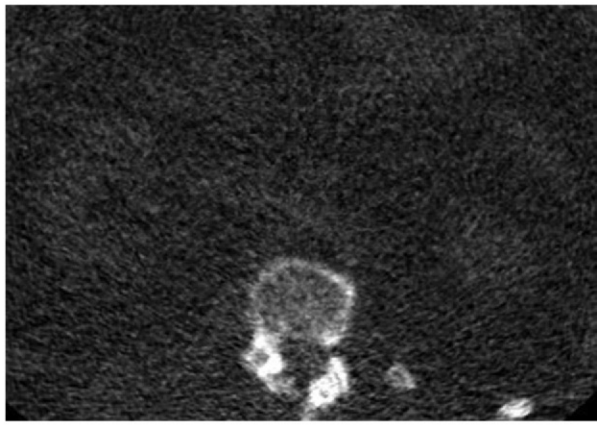

10b.

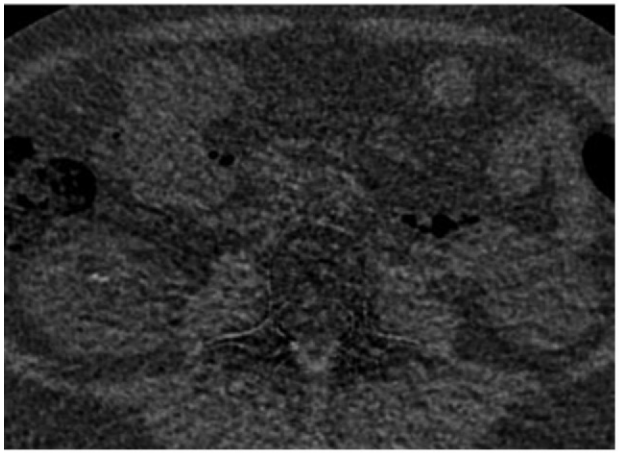

9c.

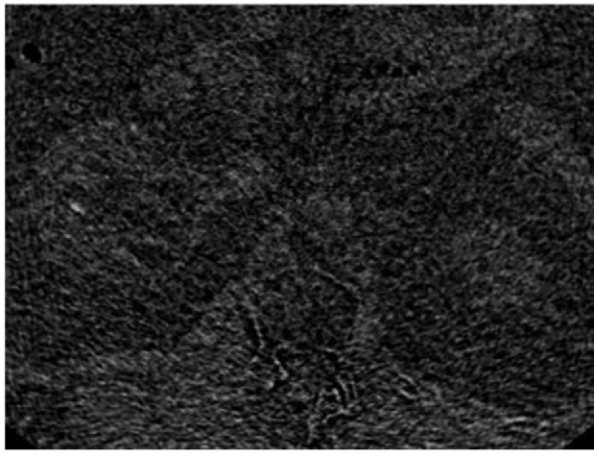

10c.

Figures 9, 10. **(9)** Calcium-containing calculus. Axial monochromatic 75-keV image **(a)** from unenhanced dual-energy CT shows a 1-cm calculus in the right kidney. **(b, c)** Calcium hydroxyapatite–density **(b)** and uric acid–density **(c)** images from the same dual-energy CT dataset as in **a** show that the calculus is conspicuous in **b** but barely visible in **c**, findings indicative of predominant calcium content. Note the similarly dark appearance of the adjacent vertebral body in **c**. **(10)** Uric acid–containing calculus. Axial monochromatic 75-keV image **(a)** from unenhanced dual-energy CT shows a 5-mm calculus in the right kidney. **(b, c)** Comparison of paired calcium hydroxyapatite **(b)** and uric acid **(c)** material-density images from the same dual-energy CT dataset as in **a** shows that the calculus is absent in **b** but faintly visible in **c**, findings indicative of predominant uric acid content. This conclusion was confirmed at subsequent urinalysis.

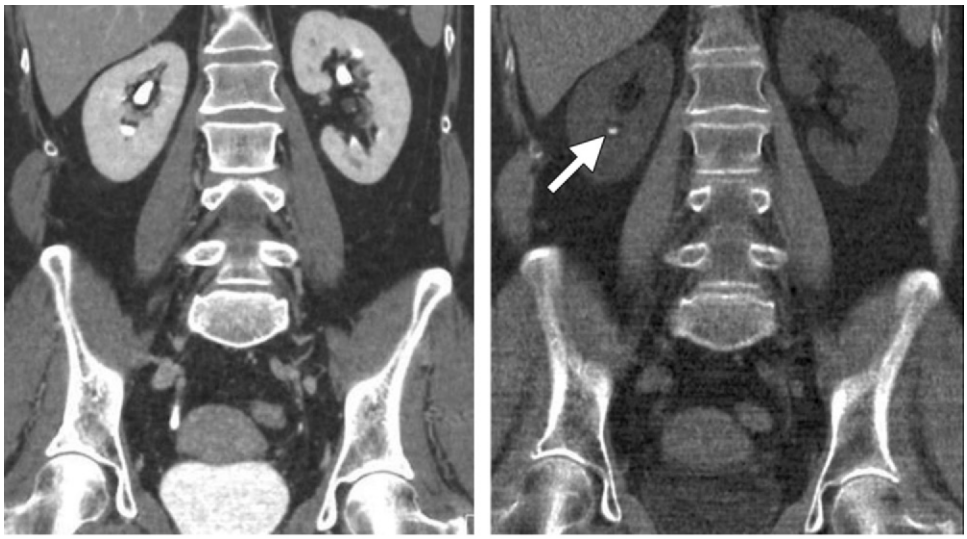

a. b.

Figure 11. **(a)** Coronal excretory-phase image from dual-energy CT urography demonstrates contrast material in the renal collecting systems and bladder. **(b)** Coronal water-density (virtual unenhanced) image obtained from the same dual-energy CT image dataset as in **a** by subtracting all iodine-containing pixels from the renal collecting systems and bladder clearly depicts a 5-mm calculus (arrow) in the lower pole of the right kidney.

calculi with great accuracy (8,9). By obtaining calcium and uric acid material-density images at dual-energy CT with fast kilovoltage switching, uric acid– and calcium-containing calculi can be differentiated, with the latter depicted on calcium-density images and the former being depicted on uric acid–density images (Figs 9, 10). Investigators also recently reported that dual-energy CT can help distinguish cystine- and struvite-containing calculi from calcium-containing calculi (10,15,25). Joshi and colleagues (25) found that when dual-energy CT is performed with fast kilovoltage switching, a plot of effective atomic numbers versus monochromatic image–based attenuation values can help distinguish among all four major categories of calculi (calcium, uric acid, struvite, and cystine); however, larger clinical studies are needed to verify their findings. To our knowledge, no published studies have directly compared the characterization of urinary tract stones according to their attenuation measurements at single-energy CT versus dual-energy CT; however, initial results obtained with the use of dual-energy CT suggest that it provides an incremental benefit for the characterization of renal stones.

CT Urography

The use of CT urography to evaluate the upper urinary tract in patients with hematuria is well established (34). All CT urography protocols include unenhanced scanning for detection of urinary tract calculi, followed by contrast-enhanced scanning in at least one phase (eg, excretory phase) for evaluation of the renal parenchyma and urothelium. With the ability to generate virtual unenhanced images from contrast-enhanced dual-energy CT image datasets, dual-energy CT urography can lessen the need for an unenhanced scanning phase (Fig 11). However, stones may be less well depicted on virtual unenhanced images than on actual unenhanced CT images. Takahashi and colleagues (35) reported that on virtual unenhanced images from excretory-phase CT urography performed with a dual-source dual-energy scanner, the rate of detection of urinary tract stones was 100% for stones larger than 7 mm but decreased progressively for smaller stones, falling to 29% for stones that were 1–2 mm in maximal diameter (Fig 12).

Teaching Point

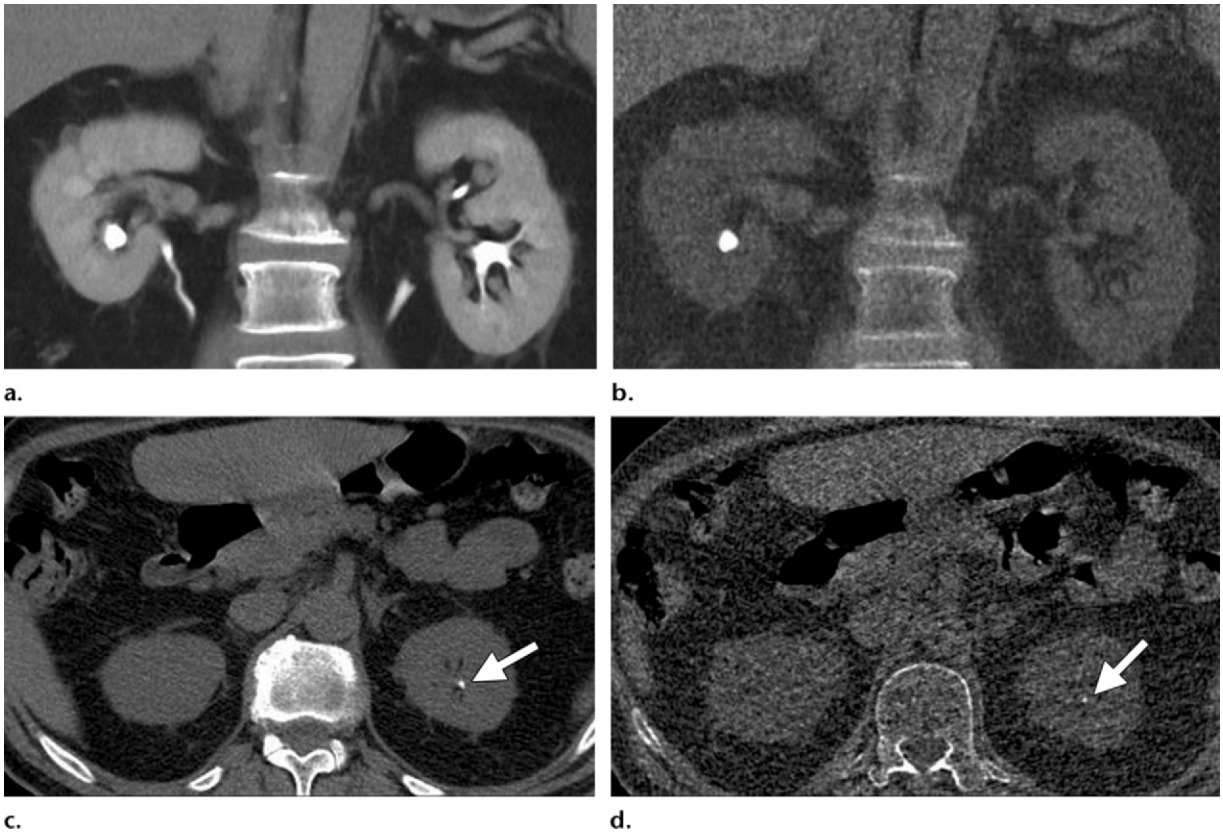

Figure 12. **(a)** Coronal excretory-phase image from dual-energy CT urography shows contrast material in both renal collecting systems. **(b)** Coronal water-density image obtained from the same CT image dataset as in **a** by subtracting all iodine-containing pixels shows a 7-mm calculus in the lower pole of the right kidney. **(c)** Axial unenhanced conventional CT image obtained in the same patient shows a 1-mm calculus (arrow) in the upper pole of the left kidney. **(d)** Axial water-density (virtual unenhanced) image from dual-energy CT, obtained at approximately the same level as **c**, shows only faint visibility of the calculus (arrow), which is nearly obscured by image noise. Renal calculi with a maximal diameter of less than 3 mm are difficult to detect on virtual unenhanced images because of high image noise levels.

A factor limiting the usefulness of virtual unenhanced images in CT urography is incomplete subtraction of the highly concentrated iodinated contrast material excreted in urine. A resultant "rim artifact" along the margins of the collecting system can obscure calculi, leading to false-negative findings; alternatively, foci of unsubtracted iodine may be mistaken for renal calculi, with resultant false-positive findings (Fig 13) (35). To overcome this limitation, it has been proposed that the CT urography protocol be modified to ensure a lower concentration of iodine in the excretory system while maintaining adequate distention either by administering smaller volumes of contrast material and diuretics or by aggressively hydrating the patient.

Offsetting this limitation somewhat is the ability of dual-energy CT urography performed with a single delayed contrast-enhanced scanning phase to help characterize renal stones when they are detected. Wang and coworkers (36) recently reported that dual-energy CT can be used to differentiate between kidney stones containing uric acid and those without uric acid, even when iodinated contrast material is present in the collecting system. If this finding is validated in clinical studies, it will support the use of dual-energy CT urography for characterizing stones.

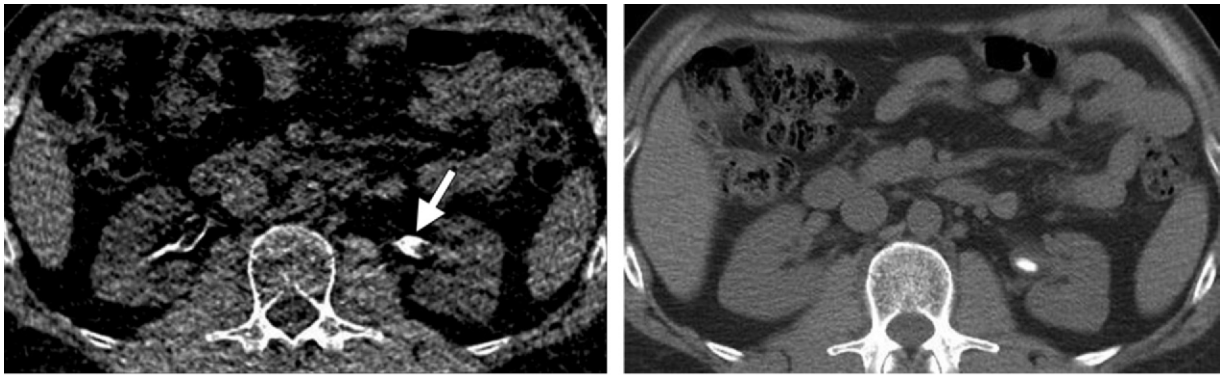

a. b.

Figure 13. **(a)** Axial water-density (virtual unenhanced) image from excretory-phase dual-energy CT urography shows a bright rim around both urinary collecting systems, an artifact that limits their visual evaluation. A focal area of hyperdensity in the left renal collecting system (arrow) might represent either an artifact or a calculus. Incomplete subtraction of iodine-containing pixels from the renal collecting systems, ureters, and bladder during the reconstruction of virtual unenhanced images may lead to both false-positive and false-negative findings of calculi. **(b)** Axial unenhanced conventional CT image helps confirm the presence of a 1-cm calculus in the left renal pelvis.

Radiation Dose Considerations

Although the results of initial studies indicated that dual-energy CT produced higher radiation doses than did single-energy CT (37), many subsequent clinical studies of dual-source dual-energy CT have shown that dual-energy CT exposes patients to radiation doses similar to those received during conventional single-energy CT (38,39). The results of more recent studies of dual-energy CT performed with fast kilovoltage switching also have shown radiation dose levels similar to those with conventional CT. Zhang and colleagues (21), in a study comparing abdominal studies performed with dual-energy CT with fast kilovoltage switching and those performed with conventional abdominal CT with a similar volume CT dose index, found that diagnostic performance based on the interpretation of 65-keV monochromatic dual-energy CT images was equivalent to that based on the interpretation of conventional CT images. In a study by Li and colleagues (13), the weighted CT dose index from dual-energy CT of the abdomen performed with fast kilovoltage switching was only 14% higher than that from conventional CT. Since virtual unenhanced images can be obtained from contrast-enhanced dual-energy CT datasets, the conventional unenhanced scanning phase can be eliminated, substantially offsetting the radiation dose difference between single- and dual-energy CT. In addition, with the further development of dual-energy CT noise-reduction algorithms, it might be possible to achieve deeper reductions in radiation dose levels. In the near future, we believe, the clinical use of dual-energy CT for abdominal imaging will no longer be hampered by concerns about increased radiation exposure. Instead, the decision to use dual-energy CT will be based entirely on the expected additional benefit in material characterization.

Advantages and Limitations of Dual-Energy CT

Dual-energy CT performed with fast kilovoltage switching has many important advantages over conventional CT for imaging of the genitourinary tract: It permits the characterization of incidental renal lesions in patients who previously underwent contrast-enhanced scanning only, thereby potentially avoiding the need for a repeat renal evaluation with both unenhanced and enhanced scanning phases. It allows the quantification of iodine content in renal lesions, information that may aid in the characterization and follow-up evaluation of renal masses, and it helps specifically characterize several different types of urinary tract calculi. In addition, it may help reduce patient radiation exposure by eliminating the need for unenhanced scanning, at least in some patients.

The limitations of dual-energy CT for genitourinary tract imaging are also potentially important. These include higher image noise on virtual unenhanced images than on actual unenhanced images; false-negative or false-positive findings of stones at CT urography because of incomplete iodine subtraction on virtual unenhanced images; the need for more time and expertise to process image data and generate images (although the time needed should decrease with increasing experience); larger image datasets requiring increased data storage capabilities; and the inability to measure attenuation in Hounsfield units on virtual unenhanced images obtained with current processing techniques. This last drawback might eventually be overcome by modified image-processing algorithms allowing the extrapolation of attenuation data.

Conclusions

The ability to obtain virtual unenhanced images and material-specific information gives dual-energy CT potential advantages over conventional CT for evaluations of the genitourinary tract. However, an understanding of the principles of dual-energy CT data processing and image generation is necessary to obtain maximal benefit from the dual-energy CT dataset. Further refinements in data processing algorithms, reductions in image noise, and modifications of dual-energy CT protocols allowing decreased radiation doses will likely lead to more widespread use of this promising technique in the near future.

***Disclosures of Potential Conflicts of Interest.*—J.F.P.:** *Related financial activities:* none. *Other financial activities:* speaker at national CT symposia. **R.H.C.:** *Related financial activities:* none. *Other financial activities:* expert witness for GE Healthcare. **R.K.K.:** *Related financial activities:* none. *Other financial activities:* speaker for GE Healthcare.

References

1. Alvarez RE, Macovski A. Energy-selective reconstructions in x-ray computerized tomography. Phys Med Biol 1976;21(5):733–744.
2. Hounsfield GN. Computerized transverse axial scanning (tomography). 1. Description of system. Br J Radiol 1973;46(552):1016–1022.
3. Kalender WA, Perman WH, Vetter JR, Klotz E. Evaluation of a prototype dual-energy computed tomographic apparatus. I. Phantom studies. Med Phys 1986;13(3):334–339.
4. Johnson TR, Krauss B, Sedlmair M, et al. Material differentiation by dual energy CT: initial experience. Eur Radiol 2007;17(6):1510–1517.
5. Fletcher JG, Takahashi N, Hartman R, et al. Dual-energy and dual-source CT: is there a role in the abdomen and pelvis? Radiol Clin North Am 2009;47(1):41–57.
6. Brown CL, Hartman RP, Dzyubak OP, et al. Dual-energy CT iodine overlay technique for characterization of renal masses as cyst or solid: a phantom feasibility study. Eur Radiol 2009;19(5):1289–1295.
7. Graser A, Johnson TR, Hecht EM, et al. Dual-energy CT in patients suspected of having renal masses: can virtual nonenhanced images replace true nonenhanced images? Radiology 2009;252(2):433–440.
8. Primak AN, Fletcher JG, Vrtiska TJ, et al. Noninvasive differentiation of uric acid versus non-uric acid kidney stones using dual-energy CT. Acad Radiol 2007;14(12):1441–1447.
9. Stolzmann P, Kozomara M, Chuck N, et al. In vivo identification of uric acid stones with dual-energy CT: diagnostic performance evaluation in patients. Abdom Imaging 2010;35(5):629–635.
10. Vrtiska TJ, Takahashi N, Fletcher JG, Hartman RP, Yu L, Kawashima A. Genitourinary applications of dual-energy CT. AJR Am J Roentgenol 2010;194(6):1434–1442.
11. Krauss B, Schmidt B, Flohr TG. Dual source CT. In: Johnson TRC, Fink C, Schönberg SO, Reiser MF, eds. Dual energy CT in clinical practice. Berlin, Germany: Springer-Verlag, 2011; 11–20.
12. Chandra N, Langan DA. Gemstone detector: dual energy imaging via fast kVp switching. In: Johnson TRC, Fink C, Schönberg SO, Reiser MF, eds. Dual energy CT in clinical practice. Berlin, Germany: Springer-Verlag, 2011; 35–41.
13. Li B, Yadava G, Hsieh J, Chandra N, Kulpins MS. Head and body $CTDI_w$ of dual-energy x-ray CT with fast-kVp switching. In: Samei E, Pelc NJ, eds. Proceedings of SPIE: medical imaging 2010. Vol 7622. Bellingham, Wash: International Society for Optical Engineering, 2010.
14. Vlassenbroek A. Dual layer CT. In: Johnson TRC, Fink C, Schönberg SO, Reiser MF, eds. Dual energy CT in clinical practice. Berlin, Germany: Springer-Verlag, 2011; 21–34.
15. Hidas G, Eliahou R, Duvdevani M, et al. Determination of renal stone composition with dual-energy CT: in vivo analysis and comparison with x-ray diffraction. Radiology 2010;257(2):394–401.

16. McCollough CH, Schmidt B, Liu X, Yu L, Leng S. Dual-energy algorithms and postprocessing techniques. In: Johnson TRC, Fink C, Schönberg SO, Reiser MF, eds. Dual energy CT in clinical practice. Berlin, Germany: Springer-Verlag, 2011; 43–51.
17. Zou YU, Silver MD. Analysis of fast kV-switching in dual energy CT using a pre-reconstruction decomposition technique. In: Hsieh J, Samei E, eds. Proceedings of SPIE: medical imaging 2008. Vol 6913. Bellingham, Wash: International Society for Optical Engineering, 2008.
18. Wu X, Langan DA, Xu D, et al. Monochromatic CT image representation via fast switching dual kVp. In: Samei E, Hsieh J, eds. Proceedings of SPIE: medical imaging 2009—physics of medical imaging. Vol 7258. Bellingham, Wash: International Society for Optical Engineering, 2009.
19. Lehmann LA, Alvarez RE, Macovski A, et al. Generalized image combinations in dual KVP digital radiography. Med Phys 1981;8(5):659–667.
20. Muller J, Vrtiska T, Schmidt B, et al. The impact of dual energy CT on pseudo enhancement of kidney lesions. In: Samei E, Pelc NJ, eds. Proceedings of SPIE: medical imaging 2010. Vol 7622. Bellingham, Wash: International Society for Optical Engineering, 2010.
21. Zhang D, Li X, Liu B. Objective characterization of GE discovery CT750 HD scanner: gemstone spectral imaging mode. Med Phys 2011;38(3): 1178–1188.
22. Coursey CA, Nelson RC, Boll DT, et al. Dual-energy multidetector CT: how does it work, what can it tell us, and when can we use it in abdominopelvic imaging? RadioGraphics 2010;30(4):1037–1055.
23. Graser A, Johnson TR, Chandarana H, Macari M. Dual energy CT: preliminary observations and potential clinical applications in the abdomen. Eur Radiol 2009;19(1):13–23.
24. Walter DJ, Tkaczyk EJ, Wu X. Accuracy and precision of dual energy CT imaging for the quantification of tissue fat content. In: Flynn MJ, Hsieh J, eds. Proceedings of SPIE: medical imaging 2006. Vol 6142. Bellingham, Wash: International Society for Optical Engineering, 2006.
25. Joshi M, Langan DA, Sahani DS, et al. Effective atomic number accuracy for kidney stone characterization using spectral CT. In: Samei E, Pelc NJ, eds. Proceedings of SPIE: medical imaging 2010. Vol 7622. Bellingham, Wash: International Society for Optical Engineering, 2010.
26. Israel GM, Bosniak MA. How I do it: evaluating renal masses. Radiology 2005;236(2):441–450.
27. Silverman SG, Israel GM, Herts BR, Richie JP. Management of the incidental renal mass. Radiology 2008;249(1):16–31.
28. Kaza RK, Caoili EM, Cohan RH, Platt JF. Distinguishing enhancing from nonenhancing renal lesions with fast kilovoltage-switching dual-energy CT. AJR Am J Roentgenol 2011 Dec;197(6):1375–1381.
29. Mendonca PRS, Bhotika R, Maddah M, et al. Multi-material decomposition of spectral CT images. In: Samei E, Pelc NJ, eds. Proceedings of SPIE: medical imaging 2010. Vol 7622. Bellingham, Wash: International Society for Optical Engineering, 2010.
30. Davenport MS, Caoili EM, Cohan RH, et al. MRI and CT characteristics of successfully ablated renal masses: imaging surveillance after radiofrequency ablation. AJR Am J Roentgenol 2009;192(6): 1571–1578.
31. Graser A, Becker CR, Staehler M, et al. Single-phase dual-energy CT allows for characterization of renal masses as benign or malignant. Invest Radiol 2010;45(7):399–405.
32. Kambadakone AR, Eisner BH, Catalano OA, Sahani DV. New and evolving concepts in the imaging and management of urolithiasis: urologists' perspective. RadioGraphics 2010;30(3):603–623.
33. Eliahou R, Hidas G, Duvdevani M, Sosna J. Determination of renal stone composition with dual-energy computed tomography: an emerging application. Semin Ultrasound CT MR 2010;31(4): 315–320.
34. Dillman JR, Caoili EM, Cohan RH. Multi-detector CT urography: a one-stop renal and urinary tract imaging modality. Abdom Imaging 2007;32(4): 519–529.
35. Takahashi N, Vrtiska TJ, Kawashima A, et al. Detectability of urinary stones on virtual nonenhanced images generated at pyelographic-phase dual-energy CT. Radiology 2010;256(1):184–190.
36. Wang J, Qu SL, McCollough CH. Differentiation of uric acid versus non-uric acid kidney stones in the presence of iodine using dual-energy CT. In: Samei E, Pelc NJ, eds. Proceedings of SPIE: medical imaging 2010. Vol 7622. Bellingham, Wash: International Society for Optical Engineering, 2010.
37. Ho LM, Yoshizumi TT, Hurwitz LM, et al. Dual energy versus single energy MDCT: measurement of radiation dose using adult abdominal imaging protocols. Acad Radiol 2009;16(11):1400–1407.
38. Thomas C, Patschan O, Ketelsen D, et al. Dual-energy CT for the characterization of urinary calculi: in vitro and in vivo evaluation of a low-dose scanning protocol. Eur Radiol 2009;19(6):1553–1559.
39. Yu L, Primak AN, Liu X, McCollough CH. Image quality optimization and evaluation of linearly mixed images in dual-source, dual-energy CT. Med Phys 2009;36(3):1019–1024.

Dual-Energy CT with Single- and Dual-Source Scanners: Current Applications in Evaluating the Genitourinary Tract

Ravi K. Kaza, MD • Joel F. Platt, MD • Richard H. Cohan, MD • Elaine M. Caoili, MD • Mahmoud M. Al-Hawary, MD • Ashish Wasnik, MD

RadioGraphics 2012; 32:353–369 • **Published online** 10.1148/rg.322115065 • **Content Codes:** CT GU PH

Page 354 (Figure on page 354)
With dual-energy CT, two image datasets are acquired in the same anatomic location with two different x-ray spectra to allow the analysis of energy-dependent changes in the attenuation of different materials (1). Each type of material demonstrates a relatively specific change in attenuation between images obtained with a high-energy spectrum and those obtained with a low-energy spectrum, and this attenuation difference allows a more nuanced characterization of the features depicted. Two different materials that show similar attenuation on images acquired with one of the two energy spectra are often more easily differentiated on images acquired with the other spectrum because of substantial differences in their attenuation (Fig 1).

Page 356
The generation of material-density images is based on the theory of basis material decomposition, which proposes that the attenuation coefficients of any material can be computed as a weighted sum of the attenuation coefficients of two basis materials as long as the k-edge of the material is not within the evaluated energy range (1,3). The two basis materials should have substantially different mass-attenuation coefficients; thus, the material pairs chosen usually differ greatly in effective atomic number.

Page 359 (Figure 3 on page 359. Figure 4 on page 360)
Paired iodine- and water-density images obtained at contrast-enhanced dual-energy CT with fast kilovoltage switching can help distinguish hyperattenuating cysts from enhancing masses without the need for an unenhanced scanning phase (Figs 3, 4) (28).

Page 363
At dual-energy CT, the change in attenuation between high- and low-energy scans can be used to differentiate types of calculi, some of which might have a similar attenuation when scanned at a single energy level (33).

Page 365 (Figure on page 365)
With the ability to generate virtual unenhanced images from contrast-enhanced dual-energy CT image datasets, dual-energy CT urography can lessen the need for an unenhanced scanning phase (Fig 11).